CHAPTER SEVEN

Finite Volume Methods via Finite Difference Methods

7.1 GENERAL

Finite volume methods (FVM), often called control volume methods, are formulated from the inner product of the governing partial differential equations with a unit function, **I**. This process results in the spatial integration of the governing equations. The integrated terms are approximated by either finite differences or finite elements, discretely summed over the entire domain. Recall that we briefly discussed this subject in Section 1.4 for one-dimensional problems.

One of the most important features of FVM is their flexibility for unstructured grids. The traditional curvilinear coordinate transformation required for FDM is no longer needed. Designation of the components of a vector normal to boundary surfaces in FVM accommodates the unstructured grid configuration with each boundary surface integral constructed between nodal points.

For illustration, consider the conservation form of the Navier-Stokes system of equations

$$\mathbf{R} = \frac{\partial \mathbf{U}}{\partial t} + \frac{\partial \mathbf{F}_i}{\partial x_i} + \frac{\partial \mathbf{G}_i}{\partial x_i} - \mathbf{B} \tag{7.1.1}$$

The finite volume equations are obtained as

$$(\mathbf{I}, \mathbf{R}) = \int_\Omega \mathbf{R}\, d\Omega = \int_\Omega \left(\frac{\partial \mathbf{U}}{\partial t} + \frac{\partial \mathbf{F}_i}{\partial x_i} + \frac{\partial \mathbf{G}_i}{\partial x_i} - \mathbf{B} \right) d\Omega = 0 \tag{7.1.2}$$

or

$$\int_\Omega \left(\frac{\partial \mathbf{U}}{\partial t} - \mathbf{B} \right) d\Omega + \int_\Gamma (\mathbf{F}_i + \mathbf{G}_i) n_i \, d\Gamma = 0 \tag{7.1.3}$$

where n_i denotes the component of a unit vector normal to the boundary surface. Discretizing (7.1.3) and summing over all discrete nodes or cells (elements) throughout the control volumes (CV) and control surfaces (CS), we obtain

$$\sum_{CV} \left(\frac{\Delta \mathbf{U}}{\Delta t} - \mathbf{B} \right) \Delta\Omega + \sum_{CS} (\mathbf{F}_i + \mathbf{G}_i) n_i \, \Delta\Gamma = 0 \tag{7.1.4}$$

or

$$\sum_{CV}(\Delta\mathbf{U}-\Delta t\mathbf{B})\Delta\Omega+\sum_{CS}\Delta t(\mathbf{F}_i+\mathbf{G}_i)n_i\Delta\Gamma=0 \tag{7.1.5}$$

The basic idea of FVM is to obtain a system of algebraic equations for the discretized control volume and control surfaces written such as in (7.1.5). In this process, the conservation of all variables is enforced across the control surfaces. Thus, when a specific quantity of a conserved variable is transported out of one control volume, the same quantity is transported into the adjacent control volumes. As a result there is no artificial creation or destruction of conserved variable. Inaccuracies that arise in coarse meshes, therefore, are not the result of a failure of any variable, but rather are due to approximation errors. Another advantage of FVM is that the discretized governing equations retain their physical interpretation, rather than possibly distorting the physics due to numerical discretization of each derivative term.

The finite volume methods are cost effective, because the calculation of flows at the surface of the adjoining control volumes need be performed only once since the expression is the same for both control volumes, differing only in sign. This gives rise to both cost reduction and algorithmic simplicity. In this chapter, finite volume methods via FDM are presented. Finite volume methods via FEM will be discussed in Chapter 15.

7.2 TWO-DIMENSIONAL PROBLEMS

There are two types of control volume formulations: the node-centered control volume and the cell (element)-centered control volume. These topics are discussed below.

7.2.1 NODE-CENTERED CONTROL VOLUME

For illustration, let us consider the two-dimensional configuration as shown in Figure 7.2.1a. Node 1 is connected to adjacent nodes 5, 7, 9, 11, and 2. The quadrilaterals A, B, C, D, and E are subdivided by connecting midpoints of lines between nodes with quadrants associated with node 1, forming the control volume for node 1 consisting of subcontrol volumes CV_1A, CV_1B, CV_1C, CV_1D, and CV_1E. Directions normal to two control surfaces of each element are identified by the arrows pointing outward, with angles $\theta^{(a)}$ and $\theta^{(b)}$ in a subcontrol volume (Figure 7.2.1b).

Let us examine the FVM formulation for the Poisson equation,

$$u_{,ii}-f=0\quad(i=1,2) \tag{7.2.1}$$

The finite volume equation becomes

$$\int_\Gamma u_{,i}n_i d\Gamma=\int_\Omega f d\Omega \tag{7.2.2}$$

or

$$\sum_{CS}^{A,B,C,D,E}\left(\frac{\Delta u}{\Delta x}n_1+\frac{\Delta u}{\Delta y}n_2\right)\Delta\Gamma=\sum_{CV}f\Delta\Omega \tag{7.2.3}$$

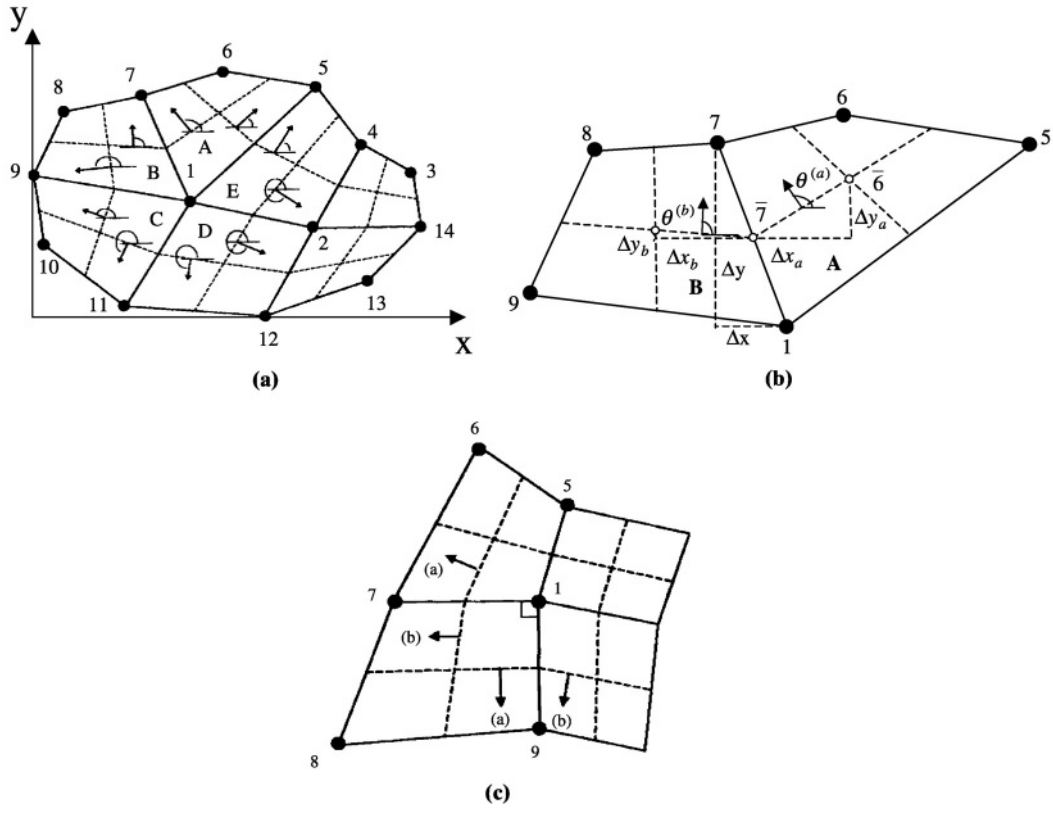

Figure 7.2.1 Control volumes and control surfaces. **(a)** Control volume at node 1 in unstructured grid system. **(b)** Control surfaces between nodes 1 and 7. **(c)** Modifications required for points 7-1 on horizontal (x) line and 9-1 on vertical (y) line.

The FDM discretization of (7.2.3) yields

$$(u_7 - u_1)S_{7,1} + (u_9 - u_1)S_{9,1} + (u_{11} - u_1)S_{11,1} + (u_2 - u_1)S_{2,1} + (u_5 - u_1)S_{5,1} = f_1\Omega_1 \tag{7.2.4}$$

with Ω_1 being the sum of the control volume areas surrounding node 1,

$$\Omega_1 = CV_1A + CV_1B + CV_1C + CV_1D + CV_1E$$

and $S_{7,1}$, $S_{9,1}$, etc. represent the surface parameters determined from the direction cosines. For example, the surface parameter $S_{7,1}$ associated with $u_7 - u_1$ is given by

$$S_{7,1} = \left(\cos\theta\frac{\Delta\Gamma}{\Delta x} + \sin\theta\frac{\Delta\Gamma}{\Delta y}\right)^{(a)}_{7,1} + \left(\cos\theta\frac{\Delta\Gamma}{\Delta x} + \sin\theta\frac{\Delta\Gamma}{\Delta y}\right)^{(b)}_{7,1} \tag{7.2.5}$$

where (a) and (b) refer to the adjacent control surfaces in the counterclockwise direction. Note also that

$$\Delta y_{(a)} = (\cos\theta\Delta\Gamma)^{(a)},\ \Delta x_{(a)} = (\sin\theta\Delta\Gamma)^{(a)}$$

refer to, respectively, the y and x components of $\Delta\Gamma$ on the control surface for the control volume A (see Figure 7.2.1b). Orientations of these surfaces are determined by the angle

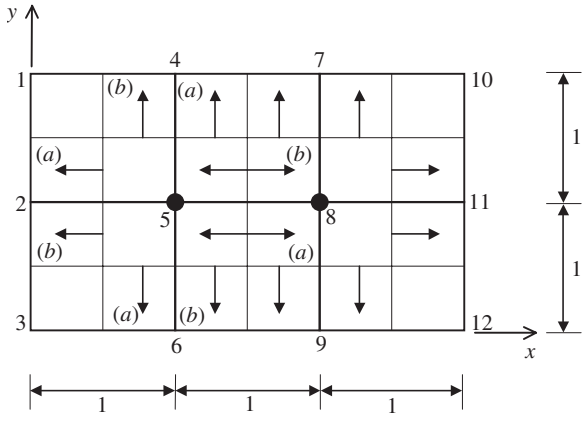

Figure E7.2.1 FVM solution of the Poisson equation.

θ of the direction cosines always measured counterclockwise from the x-axis as defined in Figure 7.2.1a. Note also that $\Delta x_{7,1} = x_7 - x_1, \Delta y_{7,1} = y_7 - y_1$, etc. It should be cautioned that, if two points are horizontal or vertical ($\Delta y = 0$ or $\Delta x = 0$), as may be the case in Figure 7.2.1c, then we set

$$\sin\theta \frac{\Delta\Gamma}{\Delta y} = 0 \quad \text{for } \Delta y = 0, \qquad \cos\theta \frac{\Delta\Gamma}{\Delta x} = 0 \quad \text{for } \Delta x = 0 \tag{7.2.6a}$$

This is to avoid division by zero ($\Delta y_{7,1} = 0, \Delta x_{9,1} = 0$). For a node in a rectangular geometry such as node 5 of Figure E7.2.1, the direction cosine is zero so that the division by zero is avoided by setting

$$\sin 180^\circ \Delta\Gamma = 0, \qquad \cos 270^\circ \Delta\Gamma = 0 \tag{7.2.6b}$$

This restriction allows the FVM formulation to yield the result identical to the FDM methods for rectangular grids. For all nonrectangular arbitrary geometries, the definitions given in (7.2.5) should be used.

Detailed computational steps for a simple geometry (Figure E7.2.1) are demonstrated in Example 7.2.1.

Example 7.2.1

Given: $\nabla^2 u = f(x, y)$, with the exact solution ($u = 2x^2y^2$), Dirichlet boundary conditions.

Required: Solve using the finite volume method via finite differences (3×2 unit square mesh, Figure E7.2.1). Dirichlet boundary data for all exterior boundaries and the source term are calculated from the exact solution.

$$u_1, u_2, u_3, u_6, u_9, u_{12} = 0$$
$$u_4 = 8, \quad u_7 = 32, \quad u_{10} = 72, \quad u_{11} = 18$$
$$f_5 = 8, \quad f_8 = 20$$

Solution:

$$\sum_{CS}\left(\frac{\Delta u}{\Delta x}n_1+\frac{\Delta u}{\Delta y}n_2\right)\Delta\Gamma=\sum_{CV}f\Delta\Omega$$

$$\sum_{CS}\Delta uS=\sum_{CV}f\Delta\Omega$$

where

$$S=\frac{n_1\,\Delta\Gamma}{\Delta x}+\frac{n_2\,\Delta\Gamma}{\Delta y}$$

We write the finite difference analogs at nodes 5 and 8 as

$$(u_2-u_5)S_{2,5}+(u_6-u_5)S_{6,5}+(u_8-u_5)S_{8.5}+(u_4-u_5)S_{4,5}=f_5A_5$$
$$(u_5-u_8)S_{5,8}+(u_9-u_8)S_{9,8}+(u_{11}-u_8)S_{11,8}+(u_7-u_8)S_{7,8}=f_8A_8$$

with

$$f_5A_5=8,\quad f_8A_8=20$$

$$S_{2,5}=\left[\left(S_{2,5}^{(1)}+S_{2,5}^{(2)}\right)^{(a)}+\left(S_{2,5}^{(1)}+S_{2,5}^{(2)}\right)^{(b)}\right]$$
$$=\left[\frac{\Delta y_{(a)}}{\Delta x_{2,5}}+0\right]+\left[\frac{\Delta y_{(b)}}{\Delta x_{2,5}}+0\right]=\left[\frac{-1/2}{-1}+0\right]+\left[\frac{-1/2}{-1}+0\right]=1$$

and

$$S_{6,5}=\left[0+\frac{\Delta x_{(a)}}{\Delta y_{6,5}}\right]+\left[0+\frac{\Delta x_{(b)}}{\Delta y_{6,5}}\right]=\left[0+\frac{-1/2}{-1}\right]+\left[0+\frac{-1/2}{-1}\right]=1$$
$$S_{8,5}=S_{4,5}=1,\quad \text{etc.}$$

Solving the above two equations for nodes 5 and 8 with the boundary conditions imposed, we obtain

$$\begin{bmatrix}-4 & 1\\ 1 & -4\end{bmatrix}\begin{bmatrix}u_5\\ u_8\end{bmatrix}=\begin{bmatrix}8-8\\ 20-50\end{bmatrix}=\begin{bmatrix}0\\ -30\end{bmatrix}$$
$$\begin{bmatrix}u_5\\ u_8\end{bmatrix}=\begin{bmatrix}2\\ 8\end{bmatrix}$$

which is the exact solution. For the structured orthogonal grids, the process is the same as in FDM.

Example 7.2.2

Given: Same as Example 7.2.1 with Neumann data:

$$\left(\frac{\partial u}{\partial x}\right)_4=16,\qquad \left(\frac{\partial u}{\partial y}\right)_4=8$$

Solution: The additional equation required at node 4 becomes

$$\left.\frac{\partial u}{\partial x}\right|_4 + \left.\frac{\partial u}{\partial y}\right|_4 + \left.\frac{\Delta u}{\Delta y}\right|_{5,4} + \left.\frac{\Delta u}{\Delta x}\right|_{1,4} + \left.\frac{\Delta u}{\Delta x}\right|_{7,4} = f_4 A_4$$

$$16 + 8 + \frac{u_{5/2} - u_4}{\Delta y/2} + \frac{u_{1/2} - u_4}{\Delta x/2} + \frac{u_{7/2} - u_4}{\Delta x/2} = 20\left(\frac{1}{2}\right)$$

Combining equations written at nodes 5 and 8 from Example 7.2.1, we obtain

$$\begin{bmatrix} -4 & 1 & 1 \\ 1 & -4 & 0 \\ 1 & 0 & -6 \end{bmatrix} \begin{bmatrix} u_5 \\ u_8 \\ u_4 \end{bmatrix} = \begin{bmatrix} 8 \\ -30 \\ -46 \end{bmatrix}$$

Thus

$$\begin{bmatrix} u_5 \\ u_8 \\ u_4 \end{bmatrix} = -\frac{1}{86} \begin{bmatrix} 24 & 6 & 4 \\ 6 & 23 & 1 \\ 4 & 1 & 15 \end{bmatrix} \begin{bmatrix} 8 \\ -30 \\ -46 \end{bmatrix} = \begin{bmatrix} 2 \\ 8 \\ 8 \end{bmatrix}$$

This is the exact solution. Note that for unstructured grids with sloped boundaries, specification of the Neumann boundary conditions must be adjusted for direction cosines.

7.2.2 CELL-CENTERED CONTROL VOLUME

In the previous section, we dealt with the case in which nodes are identified with the surrounding subcontrol volumes (node-centered control volume). Instead of subcontrol or tributary control volumes surrounding the node, it is possible to consider control volumes constructed by adjacent nodes as shown in Figure 7.2.2a,b,c. Here, control surfaces are identified between adjacent nodes for a structured grid system, leading to the cell-centered control volume. However, this requirement lacks the generality prevailing in the unstructured grid system.

For illustration, let us consider the cell-centered FVM scheme as shown in Figure 7.2.2 for the solution of the Poisson equation examined in Section 7.2.1. The corresponding FVM equation is given by (7.2.2).

$$\sum_{CS}\left(\frac{\Delta u}{\Delta x}n_1 + \frac{\Delta u}{\Delta y}n_2\right)\Delta\Gamma = \sum_{CV} f\,\Delta\Omega \tag{7.2.7}$$

This can be written for the cell-centered scheme in the form,

$$\begin{aligned}
&\left(\frac{\Delta u}{\Delta x}\right)_{i,j-1/2} n_1\Delta\Gamma_{AB} + \left(\frac{\Delta u}{\Delta y}\right)_{i,j-1/2} n_2\Delta\Gamma_{AB} + \left(\frac{\Delta u}{\Delta x}\right)_{i+1/2,j} n_1\Delta\Gamma_{BC} \\
&+ \left(\frac{\Delta u}{\Delta y}\right)_{i+1/2,j} n_2\Delta\Gamma_{BC} + \left(\frac{\Delta u}{\Delta x}\right)_{i,j+1/2} n_1\Delta\Gamma_{CD} + \left(\frac{\Delta u}{\Delta y}\right)_{i,j+1/2} n_2\Delta\Gamma_{CD} \\
&+ \left(\frac{\Delta u}{\Delta x}\right)_{i-1/2,j} n_1\Delta\Gamma_{DA} + \left(\frac{\Delta u}{\Delta y}\right)_{i-1/2,j} n_2\Delta\Gamma_{DA} = (f\Delta\Omega)_{i,j}
\end{aligned} \tag{7.2.8}$$

where $\Delta u/\Delta x$ and $\Delta u/\Delta y$ may be approximated by using tributary areas and

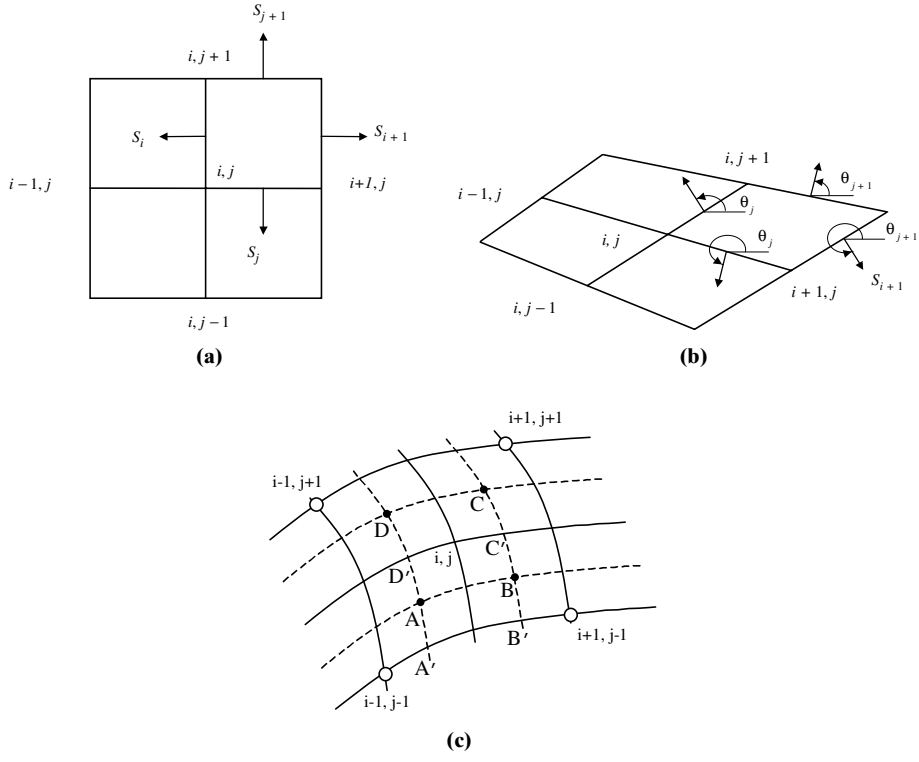

Figure 7.2.2 Cell-centered control volume. **(a)** Square or rectangular grids. **(b)** Skewed grids. **(c)** Curvilinear system.

corresponding boundary surface areas. For example, we have (Figure 7.2.2c)

$$\left(\frac{\Delta u}{\Delta x}\right)_{i,j-1/2} = \frac{1}{\Delta\Omega_{i,j-1/2}} \sum_{A'B'C'D'} u_{i,j-1/2}\Delta y_{i,j-1/2}$$
$$= (u_{i,j-1}\Delta y_{A'B'} + u_B\Delta y_{B'C'} + u_{i,j}\Delta y_{C'D'} + u_A\Delta y_{D'A'})/\Delta\Omega_{i,j-1/2}$$

with

$$u_A = \frac{1}{4}(u_{i,j} + u_{i-1,j} + u_{i-1,j-1} + u_{i,j-1})$$

$$u_B = \frac{1}{4}(u_{i,j} + u_{i+1,j} + u_{i+1,j-1} + u_{i,j-1})$$

Other quantities in (7.2.8) are calculated similarly. It can be shown that the above procedure gives the identical results for the problem in Example 7.2.1. Note that the cell-centered FVM presented here can not be applied to the unstructured grid shown in Figure 7.2.1.

The cell-centered FVM scheme for Euler equations takes the form

$$\sum_{CV}\left(\frac{\Delta \mathbf{U}}{\Delta t}\right)\Delta\Omega = -\sum_{CS}(\mathbf{F}_i S_i), \qquad S_i = n_i\Delta\Gamma \tag{7.2.9}$$

This may be solved using the operator splitting scheme or the fractional step scheme:

(1) Operator Splitting Scheme

Step 1

$$\overline{\mathbf{U}}_{i,j}^{n+1} = \mathbf{U}_{i,j}^{n} - \frac{\Delta t}{\Delta\Omega_{i,j}}\left(\mathbf{F}_{i,j}^{n} S_{j+1} + \mathbf{F}_{i,j-1}^{n} S_j + \mathbf{F}_{i,j}^{n} S_{i+1} + \mathbf{F}_{i-1,j}^{n} S_i\right) \tag{7.2.10a}$$

Step 2

$$\mathbf{U}_{i,j}^{n+1} = \frac{1}{2}\left[\mathbf{U}_{i,j}^{n} + \overline{\mathbf{U}}_{i,j}^{n+1} - \frac{\Delta t}{\Delta\Omega_{i,j}}\left(\overline{\mathbf{F}}_{i,j+1}^{n+1} S_{j+1} + \overline{\mathbf{F}}_{i,j}^{n+1} S_j + \overline{\mathbf{F}}_{i+1,j}^{n+1} S_{i+1} + \overline{\mathbf{F}}_{i,j}^{n+1} S_i\right)\right] \tag{7.2.10b}$$

These steps are repeated until steady-state is reached.

(2) Fractional Step Scheme

In this scheme, a half-time step is introduced in order to increase accuracy.

Step 1

$$\overline{\mathbf{U}}_{i,j}^{n+\frac{1}{2}} = \mathbf{U}_{i,j}^{n} - \frac{\Delta t}{\Delta\Omega_{i,j}}\left(\mathbf{F}_{i,j}^{n} S_{j+1} + \mathbf{F}_{i,j-1}^{n} S_j\right) \tag{7.2.11a}$$

$$\mathbf{U}_{i,j}^{n+\frac{1}{2}} = \frac{1}{2}\left[\mathbf{U}_{i,j}^{n} + \overline{\mathbf{U}}_{i,j}^{n+\frac{1}{2}} - \frac{\Delta t}{\Delta\Omega_{i,j}}\left(\overline{\mathbf{F}}_{i,j+1}^{n+\frac{1}{2}} S_{j+1} + \overline{\mathbf{F}}_{i,j}^{n+\frac{1}{2}} S_j\right)\right] \tag{7.2.11b}$$

Step 2

$$\overline{\mathbf{U}}_{i,j}^{n+1} = \mathbf{U}_{i,j}^{n+\frac{1}{2}} - \frac{\Delta t}{\Delta\Omega_{i,j}}\left(\mathbf{F}_{i,j}^{n+\frac{1}{2}} S_{i+1} + \mathbf{F}_{i-1,j}^{n+\frac{1}{2}} S_i\right) \tag{7.2.11c}$$

$$\mathbf{U}_{i,j}^{n+1} = \frac{1}{2}\left[\mathbf{U}_{i,j}^{n+\frac{1}{2}} + \overline{\mathbf{U}}_{i,j}^{n+1} - \frac{\Delta t}{\Delta\Omega_{i,j}}\left(\overline{\mathbf{F}}_{i+1,j}^{n+1} S_{i+1} + \overline{\mathbf{F}}_{i,j}^{n+1} S_i\right)\right] \tag{7.2.11d}$$

Here, S_i, S_{i+1}, S_j, S_{j+1} are the control surfaces as oriented by the direction cosine components in the structured grid system.

7.2.3 CELL-CENTERED AVERAGE SCHEME

The cell-centered average scheme was proposed by Ni [1982]. To illustrate, we consider the Euler equation written in the form

$$\frac{\partial \mathbf{U}}{\partial t} = -\frac{\partial \mathbf{F}}{\partial x} - \frac{\partial \mathbf{G}}{\partial y}$$

where

$$\mathbf{U} = \begin{bmatrix} \rho \\ \rho u \\ \rho \mathrm{v} \\ \rho E \end{bmatrix} \qquad \mathbf{F} = \begin{bmatrix} \rho u \\ p + \rho u^2 \\ \rho u \mathrm{v} \\ \rho E u + p u \end{bmatrix} \qquad \mathbf{G} = \begin{bmatrix} \rho \mathrm{v} \\ \rho \mathrm{v} u \\ p + \rho \mathrm{v}^2 \\ \rho E \mathrm{v} + p \mathrm{v} \end{bmatrix}$$

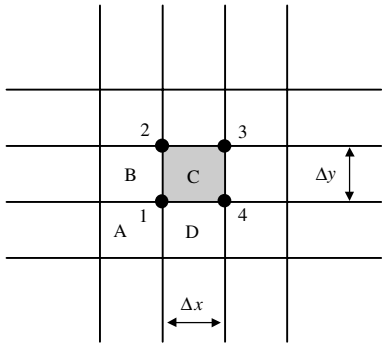

Figure 7.2.3 Cell-centered average scheme.

The control volumes for two-dimensional problems are shown in Figure 7.2.3. The change of flow variables $\mathbf{U}_c$ for the control volume C is given by

$$\Delta\mathbf{U}_c = \frac{\Delta t}{2\Delta x\Delta y}[(F_1+F_2)\Delta y-(F_3+F_4)\Delta y+(G_1+G_4)\Delta x-(G_2+G_3)\Delta x] \tag{7.2.12}$$

The corrections to the grid points associated with the control volume C (distribution formula) are determined by

$$\begin{aligned}
(\delta\mathbf{U}_1)_c &= \frac{1}{4}\left[\Delta\mathbf{U}_c-\frac{\Delta t}{\Delta x}\Delta\mathbf{F}_c-\frac{\Delta t}{\Delta y}\Delta\mathbf{G}_c\right]\\
(\delta\mathbf{U}_2)_c &= \frac{1}{4}\left[\Delta\mathbf{U}_c-\frac{\Delta t}{\Delta x}\Delta\mathbf{F}_c+\frac{\Delta t}{\Delta y}\Delta\mathbf{G}_c\right]\\
(\delta\mathbf{U}_3)_c &= \frac{1}{4}\left[\Delta\mathbf{U}_c+\frac{\Delta t}{\Delta x}\Delta\mathbf{F}_c+\frac{\Delta t}{\Delta y}\Delta\mathbf{G}_c\right]\\
(\delta\mathbf{U}_4)_c &= \frac{1}{4}\left[\Delta\mathbf{U}_c+\frac{\Delta t}{\Delta x}\Delta\mathbf{F}_c-\frac{\Delta t}{\Delta y}\Delta\mathbf{G}_c\right]
\end{aligned} \tag{7.2.13}$$

where

$$\Delta\mathbf{F}_c=\left(\frac{\partial\mathbf{F}}{\partial\mathbf{U}}\right)_c\Delta\mathbf{U}_c,\qquad \Delta\mathbf{G}_c=\left(\frac{\partial\mathbf{G}}{\partial\mathbf{U}}\right)_c\Delta\mathbf{U}_c \tag{7.2.14}$$

and

For arbitrary curvilinear coordinates, the change of flow variables for the control volume C takes the form

$$\begin{aligned}
\Delta U_c = \frac{\Delta t}{\Delta\Omega}\Bigg\{&\left[\frac{F_1+F_2}{2}(y_2-y_1)-\frac{G_1+G_2}{2}(x_2-x_1)\right]\\
&-\left[\frac{F_3+F_4}{2}(y_3-y_4)-\frac{G_3+G_4}{2}(x_3-x_4)\right]\\
&+\left[\frac{G_1+G_4}{2}(x_4-x_1)-\frac{F_1+F_4}{2}(y_4-y_1)\right]\\
&-\left[\frac{G_2+G_3}{2}(x_3-x_2)-\frac{F_2+F_3}{2}(y_3-y_2)\right]\Bigg\}
\end{aligned} \tag{7.2.15}$$

with

$$\Delta\Omega = -\frac{1}{2}[(x_3 - x_1)(y_4 - y_2) - (x_4 - x_2)(y_3 - y_1)] \tag{7.2.16}$$

The flow variables at point 1 are updated as

$$\mathbf{U}_1^{n+1} = \mathbf{U}_1^n + \delta\mathbf{U}_1 \tag{7.2.17}$$

with

$$\delta\mathbf{U}_1 = (\delta\mathbf{U}_1)_A + (\delta\mathbf{U}_1)_B + (\delta\mathbf{U}_1)_C + (\delta\mathbf{U}_1)_D \tag{7.2.18}$$

where A through D refer to control volumes surrounding the grid point 1. Here the CFL condition is given by

$$\Delta t \leq \min\left(\frac{\Delta x}{|u| + a}, \frac{\Delta y}{|\mathrm{v}| + a}\right) \tag{7.2.19}$$

It should be noted that, for transonic and supersonic flows, an artificial viscosity must be added for stability. For example,

$$(\delta\mathbf{U}_1)_c = \frac{1}{4}\left[\Delta\mathbf{U}_c - \frac{\Delta t}{\Delta x}\Delta\mathbf{F}_c - \frac{\Delta t}{\Delta y}\Delta\mathbf{G}_c + \mu(\overline{\mathbf{U}} - \mathbf{U}_1)\right] \tag{7.2.20}$$

with

$$\overline{\mathbf{U}} = \frac{1}{4}(\mathbf{U}_1 + \mathbf{U}_2 + \mathbf{U}_3 + \mathbf{U}_4) \tag{7.2.21}$$

$$\mu = \sigma\left(\frac{\Delta t}{\Delta x} + \frac{\Delta t}{\Delta y}\right) \tag{7.2.22}$$

where σ is an artificial damping factor usually taken as $0 < \sigma < 0.1$.

It is seen that the corrections defined in (7.2.13) together with (7.2.20) guarantee the proper domain of dependence regardless of local flow direction and wave speed, leading to a stable second order solution.

7.3 THREE-DIMENSIONAL PROBLEMS

7.3.1 3-D GEOMETRY DATA STRUCTURE

For three-dimensional problems dealing with arbitrary unstructured meshes, an efficient algorithm for data structure will be important. For illustration, consider the geometry shown in Figure 7.3.1, where all nodes are on the exterior global boundaries except two interior nodes, 10 and 11. The control volume for node 10 and its control surfaces are represented in Figure 7.3.2. Let us examine any inclined control surface arbitrarily located in three-dimensional reference coordinates (x, y, z) as shown in Figure 7.3.3. Note that local cartesian coordinates (x', y', z') are constructed such that the $x' - y'$ plane coincide with the control surface. The origin is located at node 1 with the x' axis lying on the line connecting nodes 1 and 2. The z' axis is in the direction of the unit vector $\mathbf{n}$ normal to the control surface. The y' axis can be determined once the unit normal vector is known. The origin of natural or isoparametric coordinates (ξ, η)

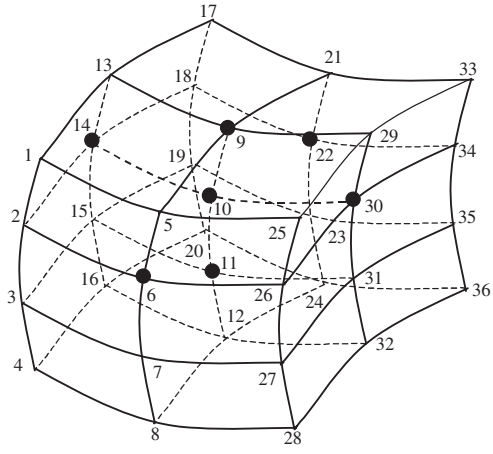

Figure 7.3.1 Illustration of 3-D finite volume discretization, 2 interior nodes 10 and 11; all other nodes are on the boundaries.

may be embedded at the controid of the quadrilateral so that the surface area can be calculated easily.

The unit vector normal to the surface is found by establishing the unit vectors $\mathbf{e}_{12}$ and $\mathbf{e}_{14}$ along the lines 1-2 and 1-4, respectively, as follows. Between nodes 1 and 2, we have

$$\mathbf{e}_{12} = \lambda_i \mathbf{i}_i \tag{7.3.1}$$

where

$$\lambda_1 = \frac{x_{12}}{L_{12}}, \quad \lambda_2 = \frac{y_{12}}{L_{12}}, \quad \lambda_3 = \frac{z_{12}}{L_{12}}$$
$$L_{12} = \left(x_{12}^2 + y_{12}^2 + z_{12}^2\right)^{1/2}$$

with $x_{12} = x_1 - x_2$, etc. Similarly, for the unit vector along the line on nodes 1 and 4, we have

$$\mathbf{e}_{14} = \mu_i \mathbf{i}_i \tag{7.3.2}$$

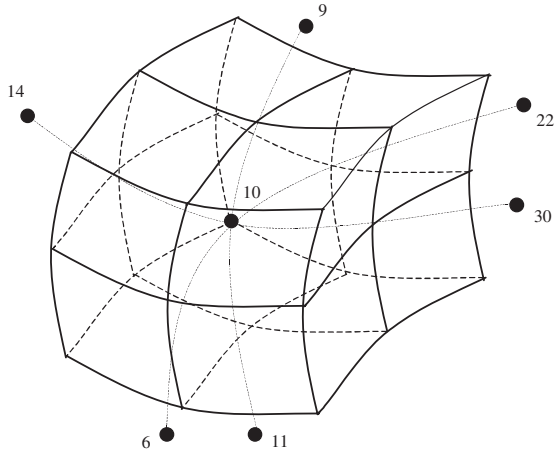

Figure 7.3.2 Control volumes and control surfaces for the interior node 10; connected neighboring nodes are 6, 14, 22, 30, 9, and 11.

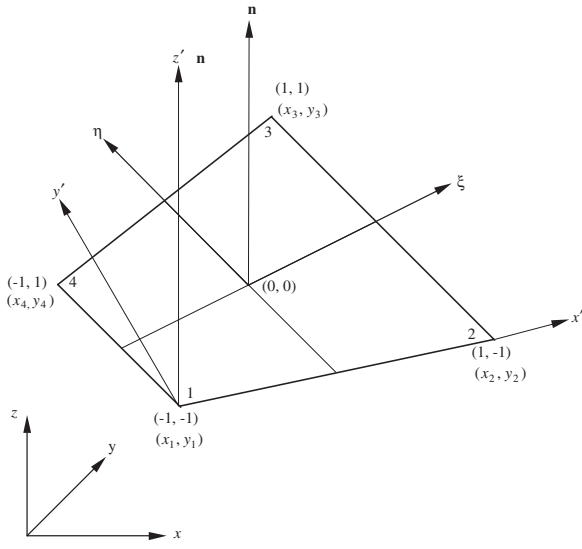

Figure 7.3.3 Control surface on the natural (isoparameteric) coordinates (ξ, η), oriented in terms of the local cartesian coordinates (x', y', z'), the unit normal vector coinciding with the z' axis.

where

$$\mu_1 = \frac{x_{14}}{L_{14}}, \qquad \mu_2 = \frac{y_{14}}{L_{14}}, \qquad \mu_3 = \frac{z_{14}}{L_{14}}$$

$$L_{14} = \left(x_{14}^2 + y_{14}^2 + z_{14}^2\right)^{1/2}$$

with $x_{14} = x_1 - x_4$, etc.

The unit vector normal to the surface is given by the cross product of these two unit vectors along the lines 1-2 and 1-4.

$$\mathbf{n} = \mathbf{e}_{12} \times \mathbf{e}_{14} = \varepsilon_{ijk}\lambda_i\mu_j\mathbf{i}_k = n_k\mathbf{i}_k \tag{7.3.3}$$

with

$$n_1 = \lambda_2\mu_3 - \lambda_3\mu_2$$
$$n_2 = \lambda_3\mu_1 - \lambda_1\mu_3$$
$$n_3 = \lambda_1\mu_2 - \lambda_2\mu_1$$

To calculate the control surface areas surrounding the control volume such as in Figure 7.3.3, it is necessary to carry out the coordinate transformation between the local coordinates (x', y', z') and the global reference coordinates (x, y, z), since the control surface plane is located arbitrarily in the three-dimensional configurations.

$$x_i' = a_{ij}x_j \tag{7.3.4}$$

where a_{ij} is the transformation matrix. The components of a_{ij} corresponding to the x_1' are the same as those for the unit vector $\mathbf{e}_{12}$,

$$a_{11} = \lambda_1, \quad a_{12} = \lambda_2, \quad a_{13} = \lambda_3$$

To determine the rest of the direction cosines, we must find the unit vector along the

y' axis. This can be done by the cross product of the normal vector (7.3.3) and the unit vector along the 1-2 direction,

$$\mathbf{e}_y = \mathbf{n} \times \mathbf{e}_{12} = \varepsilon_{ijk} n_i \lambda_j \mathbf{i}_k = \gamma_k \mathbf{i}_k \tag{7.3.5}$$

with

$$\gamma_1 = n_2\lambda_3 - n_3\lambda_2$$
$$\gamma_2 = n_3\lambda_1 - n_1\lambda_3$$
$$\gamma_3 = n_1\lambda_2 - n_2\lambda_1$$

Thus, we have

$$a_{21} = \gamma_1, \qquad a_{22} = \gamma_2, \qquad a_{23} = \gamma_3$$
$$a_{31} = n_1, \qquad a_{32} = n_2, \qquad a_{33} = n_3$$

The remaining task for the construction of data structure is the calculation of control surface areas and control volumes.

Control Surface Area

$$A = \iint dx'dy' = \int_{-1}^{1}\int_{-1}^{1} |J'| d\xi d\eta \tag{7.3.6}$$

with $|J'|$ being the determinant of the control surface Jacobian (see Section 9.3.3 for derivation),

$$|J'| = \begin{vmatrix} \dfrac{\partial x'}{\partial \xi} & \dfrac{\partial y'}{\partial \xi} \\ \dfrac{\partial x'}{\partial \eta} & \dfrac{\partial y'}{\partial \eta} \end{vmatrix} \tag{7.3.7}$$

$$x' = a_{11}x + a_{12}y + a_{13}z \tag{7.3.8}$$
$$y' = a_{21}x + a_{22}y + a_{23}z$$

$$x = \Phi_N(\xi, \eta) x_N \quad (N = 1, 2, 3, 4) \tag{7.3.9}$$

$$\Phi_1 = \frac{1}{4}(1-\xi)(1-\eta), \qquad \Phi_2 = \frac{1}{4}(1+\xi)(1-\eta), \qquad \Phi_3 = \frac{1}{4}(1+\xi)(1+\eta),$$
$$\Phi_4 = \frac{1}{4}(1-\xi)(1+\eta) \tag{7.3.10}$$

with Φ_N being the interpolation functions derived in Section 9.3.3. Substituting (7.3.10) into (7.3.9), (7.3.8), and (7.3.7), we obtain

$$\begin{aligned}
\frac{\partial x'}{\partial \xi} &= a_{11}\frac{\partial \Phi_N}{\partial \xi}x_N + a_{12}\frac{\partial \Phi_N}{\partial \xi}y_N + a_{13}\frac{\partial \Phi_N}{\partial \xi}z_N \\
\frac{\partial y'}{\partial \xi} &= a_{21}\frac{\partial \Phi_N}{\partial \xi}x_N + a_{22}\frac{\partial \Phi_N}{\partial \xi}y_N + a_{23}\frac{\partial \Phi_N}{\partial \xi}z_N \\
\frac{\partial x'}{\partial \eta} &= a_{11}\frac{\partial \Phi_N}{\partial \eta}x_N + a_{12}\frac{\partial \Phi_N}{\partial \eta}y_N + a_{13}\frac{\partial \Phi_N}{\partial \eta}z_N \\
\frac{\partial y'}{\partial \eta} &= a_{21}\frac{\partial \Phi_N}{\partial \eta}x_N + a_{22}\frac{\partial \Phi_N}{\partial \eta}y_N + a_{23}\frac{\partial \Phi_N}{\partial \eta}z_N
\end{aligned} \tag{7.3.11}$$

Integration of (7.3.6) can be carried out most accurately by using the Gaussian quadrature, which is detailed in Section 9.3.3.

Control Volume

$$V = \iiint dxdydz = \int_{-1}^{1}\int_{-1}^{1}\int_{-1}^{1} |J| d\xi d\eta d\zeta \tag{7.3.12}$$

$$|J| = \begin{vmatrix} \frac{\partial x}{\partial \xi} & \frac{\partial y}{\partial \xi} & \frac{\partial z}{\partial \xi} \\ \frac{\partial x}{\partial \eta} & \frac{\partial y}{\partial \eta} & \frac{\partial z}{\partial \eta} \\ \frac{\partial x}{\partial \zeta} & \frac{\partial y}{\partial \zeta} & \frac{\partial z}{\partial \zeta} \end{vmatrix} \tag{7.3.13}$$

with $|J|$ being the determinant of the control volume Jacobian in terms of the natural or isoparameteric coordinates (ξ, η, ζ) with reference to the global cartesian coordinates (x, y, z) as shown in Figure 7.3.4. See Section 9.4.3 for derivation and details of integration using the Gaussian quadrature.

The control surface and control volume for a three-dimensional geometry may be calculated alternatively as follows. Referring to Figure 7.3.5, the surface area A_{1234} is equal to one-half of the absolute value of the cross product between the diagonal unit vectors times their corresponding physical lengths.

$$A_{1234} = |\mathbf{A}_{1234}| = \frac{1}{2}|\mathbf{e}_{13} L_{13} \times \mathbf{e}_{24} L_{24}| \tag{7.3.14}$$

Here, the calculation of the components of the unit vectors follow the same procedure as in (7.3.1) and (7.3.2). These surface areas should be oriented by the unit normal vector calculated from (7.3.3).

Similarly, the control volume is equal to one third of the dot product of the sum of any three adjacent surface area vectors and the unit vector times its physical length,

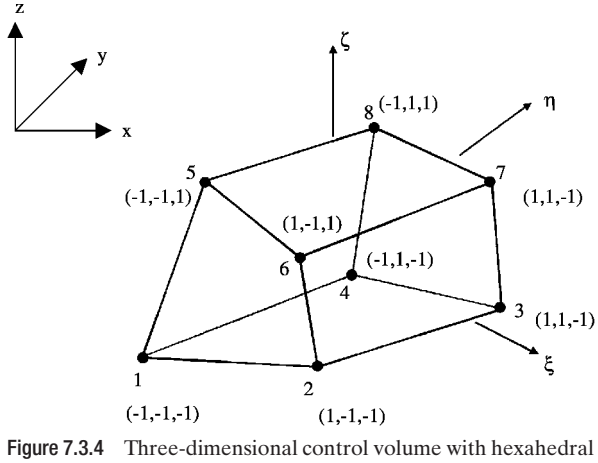

Figure 7.3.4 Three-dimensional control volume with hexahedral isoparameteric coordinates.

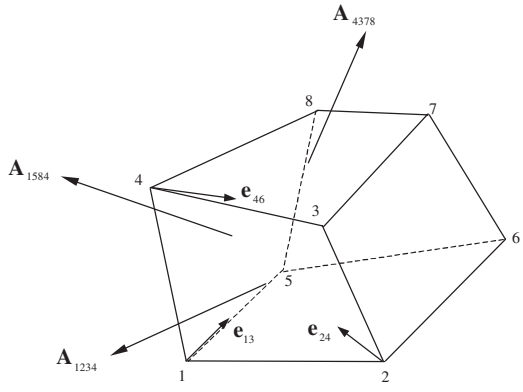

Figure 7.3.5 Alternative method for calculations of control surface areas and control volume.

connecting two nodes diagonally with one of them containing the three surfaces under consideration.

$$V = \frac{1}{3}(\mathbf{A}_{1234} + \mathbf{A}_{4378} + \mathbf{A}_{1584}) \cdot \mathbf{e}_{46} L_{46}$$
$$= \frac{1}{3}(\mathbf{e}_{13} L_{13} \times \mathbf{e}_{24} L_{24} + \mathbf{e}_{47} L_{47} \times \mathbf{e}_{38} L_{38} + \mathbf{e}_{18} L_{18} \times e_{54} L_{54}) \cdot \mathbf{e}_{46} L_{46} \qquad (7.3.15)$$

in which node 4 is common to the three surfaces and node 6 is in the diagonal direction constituting the unit vector $\mathbf{e}_{46}$, with all unit vectors calculated similarly as in (7.3.1).

7.3.2 THREE-DIMENSIONAL FVM EQUATIONS

Three-dimensional FVM via FDM can be formulated as a direct extension of the two-dimensional case discussed in Section 7.2. A typical control volume element configuration is shown in Figure 7.3.6. The cell-centered control volume procedure for the Euler

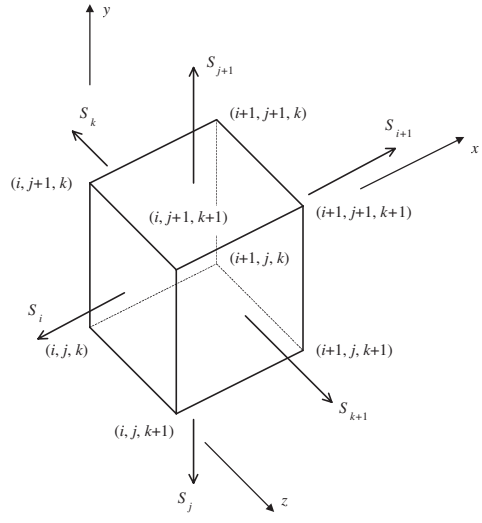

Figure 7.3.6 Three-dimensional discretization.

equation using the operator splitting and fractional step scheme is described below [Rizzi and Inouye, 1973].

(1) Operator Splitting Scheme

Step 1

$$\overline{\mathbf{U}}^{n+1}_{i,j,k} = \mathbf{U}^{n}_{i,j,k} - \frac{\Delta t}{\Delta\Omega_{i,j,k}}\left(\mathbf{F}^{n}_{i,j,k}S_{j+1} + \mathbf{F}^{n}_{i,j-1,k}S_j + \mathbf{F}^{n}_{i,j,k}S_{i+1} + \mathbf{F}^{n}_{i-1,j,k}S_i + \mathbf{F}^{n}_{i,j,k}S_{k+1} + \mathbf{F}^{n}_{i,j,k-1}S_k\right) \tag{7.3.16a}$$

Step 2

$$\mathbf{U}^{n+1}_{i,j,k} = \frac{1}{2}\left[\mathbf{U}^{n}_{i,j,k} + \overline{\mathbf{U}}^{n+1}_{i,j,k} - \frac{\Delta t}{\Delta\Omega_{i,j,k}}\left(\overline{\mathbf{F}}^{n+1}_{i,j+1,k}S_{j+1} + \overline{\mathbf{F}}^{n+1}_{i,j,k}S_j + \overline{\mathbf{F}}^{n+1}_{i+1,j,k}S_{i+1} + \overline{\mathbf{F}}^{n+1}_{i,j,k}S_i + \overline{\mathbf{F}}^{n+1}_{i,j,k+1}S_{k+1} + \overline{\mathbf{F}}^{n+1}_{i,j,k}S_k\right)\right] \tag{7.3.16b}$$

(2) Fractional Step Scheme

Step 1

$$\overline{\mathbf{U}}^{n+\frac{1}{3}}_{i,j,k} = \mathbf{U}^{n}_{i,j,k} - \frac{\Delta t}{\Delta\Omega_{i,j,k}}\left(\mathbf{F}^{n}_{i,j,k}S_{j+1} + \mathbf{F}^{n}_{i,j-1,k}S_j\right) \tag{7.3.17a}$$

$$\mathbf{U}^{n+\frac{1}{3}}_{i,j,k} = \frac{1}{2}\left[\mathbf{U}^{n}_{i,j,k} + \overline{\mathbf{U}}^{n+\frac{1}{3}}_{i,j,k} - \frac{\Delta t}{\Delta\Omega_{i,j,k}}\left(\overline{\mathbf{F}}^{n+\frac{1}{3}}_{i,j+1,k}S_{j+1} + \overline{\mathbf{F}}^{n+\frac{1}{3}}_{i,j,k}S_j\right)\right] \tag{7.3.17b}$$

Step 2

$$\overline{\mathbf{U}}^{n+\frac{2}{3}}_{i,j,k} = \mathbf{U}^{n+\frac{1}{3}}_{i,j,k} - \frac{\Delta t}{\Delta\Omega_{i,j,k}}\left(\mathbf{F}^{n+\frac{1}{3}}_{i,j,k}S_{i+1} + \mathbf{F}^{n+\frac{1}{3}}_{i-1,j,k}S_i\right) \tag{7.3.18a}$$

$$\mathbf{U}^{n+\frac{2}{3}}_{i,j,k} = \frac{1}{2}\left[\mathbf{U}^{n+\frac{1}{3}}_{i,j,k} + \overline{\mathbf{U}}^{n+\frac{2}{3}}_{i,j,k} - \frac{\Delta t}{\Delta\Omega_{i,j,k}}\left(\overline{\mathbf{F}}^{n+\frac{2}{3}}_{i+1,j,k}S_{i+1} + \overline{\mathbf{F}}^{n+\frac{2}{3}}_{i,j,k}S_i\right)\right] \tag{7.3.18b}$$

Step 3

$$\overline{\mathbf{U}}^{n+1}_{i,j,k} = \mathbf{U}^{n+\frac{2}{3}}_{i,j,k} - \frac{\Delta t}{\Delta\Omega_{i,j,k}}\left(\mathbf{F}^{n+\frac{2}{3}}_{i,j,k}S_{k+1} + \mathbf{F}^{n+\frac{2}{3}}_{i,j,k-1}S_k\right) \tag{7.3.19a}$$

$$\mathbf{U}^{n+1}_{i,j,k} = \frac{1}{2}\left[\mathbf{U}^{n+\frac{2}{3}}_{i,j,k} + \overline{\mathbf{U}}^{n+1}_{i,j,k} - \frac{\Delta t}{\Delta\Omega_{i,j,k}}\overline{\mathbf{F}}^{n+1}_{i,j,k+1}S_{k+1} + \overline{\mathbf{F}}^{n+1}_{i,j,k}S_k\right] \tag{7.3.19b}$$

Stability conditions may be given as

$$\Delta t \le \min\left(\Delta t_x,\ \Delta t_y,\ \Delta t_z\right) \tag{7.3.20}$$

with

$$\Delta t_x \le \min_{i,j,k}\left[\frac{\Delta\Omega_{i,j,k}}{\left(|\mathbf{q}\cdot\mathbf{S}_i| + aS_i\right)_{i,j,k}}\right] \tag{7.3.21a}$$

$$\Delta t_y \le \min_{i,j,k}\left[\frac{\Delta\Omega_{i,j,k}}{(|\mathbf{q}\cdot\mathbf{S}_j| + aS_j)_{i,j,k}}\right] \tag{7.3.21b}$$

$$\Delta t_z \le \min_{i,j,k}\left[\frac{\Delta\Omega_{i,j,k}}{(|\mathbf{q}\cdot\mathbf{S}_k| + aS_k)_{i,j,k}}\right] \tag{7.3.21c}$$

where $\mathbf{q}$ and a are the resultant velocity vector and speed of sound, respectively.

The node-centered control volume approach as demonstrated for two dimensions may also be used for three dimensions. We discuss this subject for the FDV equations in the following section.

7.4 FVM-FDV FORMULATION

The FDV concept introduced in Section 6.5 can be used for the FVM formulation. To this end, we begin with the FDV governing equations given by (6.5.14)

$$\mathbf{R} = \left(\mathbf{I} + \mathbf{E}_i^n\frac{\partial}{\partial x_i} + \mathbf{E}_{ij}^n\frac{\partial^2}{\partial x_i\partial x_j}\right)\Delta\mathbf{U}^{n+1} + \mathbf{Q}^n \tag{7.4.1}$$

The FVM integration equation is of the form

$$\int_\Omega \mathbf{R}d\Omega = \int_\Omega\left[\left(\mathbf{I} + \mathbf{E}_i^n\frac{\partial}{\partial x_i} + \mathbf{E}_{ij}^n\frac{\partial^2}{\partial x_i\partial x_j}\right)\Delta\mathbf{U}^{n+1} + \mathbf{Q}^n\right]d\Omega = 0 \tag{7.4.2}$$

Integrating (7.4.2) with respect to the spatial coordinates, we obtain

$$\int_\Omega \Delta\mathbf{U}^{n+1}\,d\,\Omega + \int_\Gamma\left(\mathbf{E}_i\Delta\mathbf{U}^{n+1} + \mathbf{E}_{ij}\Delta\mathbf{U}_{,j}^{n+1}\right)n_i\,d\,\Gamma = -\int_\Omega \mathbf{Q}^n d\,\Omega \tag{7.4.3}$$

or

$$\sum_{CV}\Delta\mathbf{U}^{n+1}\,\Delta\,\Omega + \sum_{CS}\left(\mathbf{E}_i\Delta\mathbf{U}^{n+1} + \mathbf{E}_{ij}\Delta\mathbf{U}_{,j}^{n+1}\right)n_i\,\Delta\Gamma = -\int_\Omega \mathbf{Q}^n d\,\Omega \tag{7.4.4}$$

where

$$\int_\Omega \mathbf{Q}^n d\,\Omega = \int_\Gamma\left(\mathbf{H}_i^n + \mathbf{H}_{ij,j}^n\right)n_i\,d\,\Gamma = \sum_{CS}\left(\mathbf{H}_i^n + \mathbf{H}_{ij,j}^n\right)n_i\Delta\Gamma \tag{7.4.5}$$

with

$$\mathbf{H}_i^n = \Delta t\left(\mathbf{F}_i^n + \mathbf{G}_i^n\right), \qquad \mathbf{H}_{ij}^n = \frac{\Delta t^2}{2}(\mathbf{a}_i + \mathbf{b}_i)\left(\mathbf{F}_j^n + \mathbf{G}_j^n\right) \tag{7.4.6a,b}$$

Let us now illustrate the solution procedure (7.4.4) based on the node-centered control volume as shown in Figure 7.2.1 and Example 7.2.1. The control surface computations on the left-hand side of (7.4.4) include terms with $\mathbf{E}_i$ without derivative and those with $\mathbf{E}_{ij}$ with the first order derivatives and similarly for $\mathbf{H}_i^n$ and $\mathbf{H}_{ij}^n$ on the right-hand side of (7.4.4). Thus, the FVM equation at node 1 for Figure 7.2.1 becomes

(with $\Delta\mathbf{U}^{n+1} = \boldsymbol{\Psi}$)

$$\begin{aligned}
&\boldsymbol{\Psi}_1\Delta\Omega_1 + \frac{1}{2}(\boldsymbol{\Psi}_7 + \boldsymbol{\Psi}_1)R_{7,1} + (\boldsymbol{\Psi}_7 - \boldsymbol{\Psi}_1)S_{7,1} + \frac{1}{2}(\boldsymbol{\Psi}_9 + \boldsymbol{\Psi}_1)R_{9,1} + (\boldsymbol{\Psi}_9 - \boldsymbol{\Psi}_1)S_{9,1} \\
&\quad + \frac{1}{2}(\boldsymbol{\Psi}_{11} + \boldsymbol{\Psi}_1)R_{11,1} + (\boldsymbol{\Psi}_{11} - \boldsymbol{\Psi}_1)S_{11,1} + \frac{1}{2}(\boldsymbol{\Psi}_2 + \boldsymbol{\Psi}_1)R_{2,1} + (\boldsymbol{\Psi}_2 - \boldsymbol{\Psi}_1)S_{2,1} \\
&\quad + \frac{1}{2}(\boldsymbol{\Psi}_5 + \boldsymbol{\Psi}_1)R_{5,1} + (\boldsymbol{\Psi}_5 - \boldsymbol{\Psi}_1)S_{5,1} = -\mathbf{Q}_1
\end{aligned} \tag{7.4.7}$$

where

$$\mathbf{R}_{7,1} = \left\lfloor (\mathbf{E}_1\mathbf{n}_1\Delta\Gamma + \mathbf{E}_2\mathbf{n}_2\Delta\Gamma)^{(a)} + (\mathbf{E}_1\mathbf{n}_1\Delta\Gamma + \mathbf{E}_2\mathbf{n}_2\Delta\Gamma)^{(b)} \right\rfloor_{7,1} \tag{7.4.8}$$

$$\mathbf{S}_{7,1} = \left\{ \begin{aligned} &\left[(\mathbf{E}_{11}\mathbf{n}_1 + \mathbf{E}_{21}\mathbf{n}_2)\frac{\Delta\boldsymbol{\Gamma}}{\Delta\mathbf{x}} + (\mathbf{E}_{12}\mathbf{n}_1 + \mathbf{E}_{22}\mathbf{n}_2)\frac{\Delta\boldsymbol{\Gamma}}{\Delta\mathbf{y}} \right]^{(a)} \\ &+ \left[(\mathbf{E}_{11}\mathbf{n}_1 + \mathbf{E}_{21}\mathbf{n}_2)\frac{\Delta\boldsymbol{\Gamma}}{\Delta\mathbf{x}} + (\mathbf{E}_{12}\mathbf{n}_1 + \mathbf{E}_{22}\mathbf{n}_2)\frac{\Delta\boldsymbol{\Gamma}}{\Delta\mathbf{y}} \right]^{(b)} \end{aligned} \right\}_{7,1} \tag{7.4.9}$$

with $\mathbf{E}_i$ and $\mathbf{E}_{ij}$ given by (6.3.31a) and (6.3.31b), respectively, etc., and $\frac{1}{\Delta x}$ and $\frac{1}{\Delta y}$ calculated similarly as in (7.2.5).

The right-hand side terms of $\mathbf{H}$ are obtained in a manner similar to the left-hand side.

$$\mathbf{Q}_1 = \overline{\mathbf{R}}^n_{7,1} + \overline{\mathbf{S}}^n_{7,1} + \overline{\mathbf{R}}^n_{9,1} + \overline{\mathbf{S}}^n_{9,1} + \overline{\mathbf{R}}^n_{11,1} + \overline{\mathbf{S}}^n_{11,1} + \overline{\mathbf{R}}^n_{2,1} + \overline{\mathbf{S}}^n_{2,1} + \overline{\mathbf{R}}^n_{5,1} + \overline{\mathbf{S}}^n_{5,1} \tag{7.4.10}$$

$$\begin{aligned}
\overline{\mathbf{R}}^n_{7,1} &= \frac{1}{2}\{[(\mathbf{H}_1\mathbf{n}_1 + \mathbf{H}_2\mathbf{n}_2)\Delta\Gamma]_7 + [(\mathbf{H}_1\mathbf{n}_1 + \mathbf{H}_2\mathbf{n}_2)\Delta\Gamma]_1\}^{(a)} \\
&\quad + \frac{1}{2}\{[(\mathbf{H}_1\mathbf{n}_1 + \mathbf{H}_2\mathbf{n}_2)\Delta\Gamma]_7 + [(\mathbf{H}_1\mathbf{n}_1 + \mathbf{H}_2\mathbf{n}_2)\Delta\Gamma]_1\}^{(b)} \\
\overline{\mathbf{S}}^n_{7,1} &= \left\{ [(\mathbf{H}_{11})_7 - (\mathbf{H}_{11})_1]\mathbf{n}_1\frac{\Delta\Gamma}{\Delta\mathbf{x}} + [(\mathbf{H}_{12})_7 - (\mathbf{H}_{12})_1]\mathbf{n}_1\frac{\Delta\Gamma}{\Delta\mathbf{y}} \right. \\
&\quad \left. + [(\mathbf{H}_{21})_7 - (\mathbf{H}_{21})_1]\mathbf{n}_2\frac{\Delta\Gamma}{\Delta\mathbf{x}} + [(\mathbf{H}_{22})_7 - (\mathbf{H}_{22})_1]\mathbf{n}_2\frac{\Delta\Gamma}{\Delta\mathbf{y}} \right\}^{(a)}_{7,1} \\
&\quad + \left\{ [(\mathbf{H}_{11})_7 - (\mathbf{H}_{11})_1]\mathbf{n}_1\frac{\Delta\Gamma}{\Delta\mathbf{x}} + [(\mathbf{H}_{12})_7 - (\mathbf{H}_{12})_1]\mathbf{n}_1\frac{\Delta\Gamma}{\Delta\mathbf{y}} \right. \\
&\quad \left. + [(\mathbf{H}_{21})_7 - (\mathbf{H}_{21})_1]\mathbf{n}_2\frac{\Delta\Gamma}{\Delta\mathbf{x}} + [(\mathbf{H}_{22})_7 - (\mathbf{H}_{22})_1]\mathbf{n}_2\frac{\Delta\Gamma}{\Delta\mathbf{y}} \right\}^{(b)}_{7,1}
\end{aligned} \tag{7.4.11}$$

with $\mathbf{H}_i$ and $\mathbf{H}_{ij}$ given by (7.4.6a,b), respectively.

The FVM equation at node 2 is written similarly and the solution for $\mathbf{U}^{n+1}$ for nodes 1 and 2 can be obtained with appropriate boundary conditions applied similarly, as demonstrated in Examples 7.2.1 and 7.2.2. If all Dirichlet data are provided, then we have

$$\begin{bmatrix} \mathbf{K}_{11} & \mathbf{K}_{12} \\ \mathbf{K}_{21} & \mathbf{K}_{22} \end{bmatrix} \begin{bmatrix} \Delta\mathbf{U}_1 \\ \Delta\mathbf{U}_2 \end{bmatrix}^{n+1} = -\begin{bmatrix} \mathbf{Q}_1 \\ \mathbf{Q}_2 \end{bmatrix}^n + \begin{bmatrix} \mathbf{D}_1 \\ \mathbf{D}_2 \end{bmatrix} \tag{7.4.12}$$

where $\mathbf{D}_1$ and $\mathbf{D}_2$ represent the source vector as a result of the Dirichlet boundary

conditions. Note that $\mathbf{K}_{11}$ and $\mathbf{K}_{22}$ denote the collective sum of contributions for nodes 1 and 2, respectively, whereas $\mathbf{K}_{12}$ and $\mathbf{K}_{21}$ are the interactions between node 1 and node 2, respectively,

$$\mathbf{K}_{12} = \frac{1}{2}\mathbf{R}_{2,1} - \mathbf{S}_{2,1}$$
$$\mathbf{K}_{21} = \frac{1}{2}\mathbf{R}_{1,2} - \mathbf{S}_{1,2} \tag{7.4.13a,b}$$

Implementation of Neumann boundary conditions is carried out similarly as in Example 7.2.2. If the Neumann boundary condition is prescribed at node 7, then the FDV equations (7.4.12) will be modified to include ΔU_7 as one of the unknowns with the Neumann data directly imposed on the right-hand side of (7.4.12).

For three-dimensional applications such as in Figure 7.3.1, FDV equations in terms of FVM are written similarly as in 2-D, following the procedure of (7.4.7) through (7.4.13). For example, at node 10 (Figure 7.3.1), the adjacent nodes connected to node 10 are as shown in Figure 7.3.2. Direction cosines of the normal vector are calculated (Figure 7.3.3), with control surface areas and control volumes determined as described in Section 7.3. Let us examine the FDV finite volume equations at node 10 (Figures 7.3.1 and 7.3.2).

$$\begin{aligned}
&\Psi_{10}\Delta\Omega_{10} + \frac{1}{2}(\Psi_6 + \Psi_{10})R_{6,10} + (\Psi_6 - \Psi_{10})S_{6,10} + \frac{1}{2}(\Psi_{14} + \Psi_{10})R_{14,10} \\
&\quad + (\Psi_{14} - \Psi_{10})S_{14,10} + \frac{1}{2}(\Psi_{22} + \Psi_{10})R_{22,10} + (\Psi_{22} - \Psi_{10})S_{22,10} \\
&\quad + \frac{1}{2}(\Psi_{14} + \Psi_{10})R_{14,10} + (\Psi_{14} - \Psi_{10})S_{14,10} + \frac{1}{2}(\Psi_9 + \Psi_{10})R_{9,10} \\
&\quad + (\Psi_9 - \Psi_{10})S_{9,10} + \frac{1}{2}(\Psi_{11} + \Psi_{10})R_{11,10} + (\Psi_{11} - \Psi_{10})S_{11,10} = -\mathbf{Q}_{10}
\end{aligned} \tag{7.4.14}$$

with

$$R_{6,10} = \left[\begin{array}{l}(E_1 n_1 \Delta\Gamma + E_2 n_2 \Delta\Gamma + E_3 n_3 \Delta\Gamma)^{(a)} + (E_1 n_1 \Delta\Gamma + E_2 n_2 \Delta\Gamma + E_3 n_3 \Delta\Gamma)^{(b)} \\ + (E_1 n_1 \Delta\Gamma + E_2 n_2 \Delta\Gamma + E_3 n_3 \Delta\Gamma)^{(c)} + (E_1 n_1 \Delta\Gamma + E_2 n_2 \Delta\Gamma + E_3 n_3 \Delta\Gamma)^{(d)}\end{array}\right]_{6,10} \tag{7.4.15}$$

$$S_{6,10} = \left\{\begin{array}{l}\left[(E_{11}n_1 + E_{21}n_2 + E_{31}n_3)\frac{\Delta\Gamma}{\Delta x} + (E_{12}n_1 + E_{22}n_2 + E_{32}n_3)\frac{\Delta\Gamma}{\Delta y} + (E_{13}n_1 + E_{23}n_2 + E_{33}n_3)\frac{\Delta\Gamma}{\Delta z}\right]^{(a)} \\ + \left[(E_{11}n_1 + E_{21}n_2 + E_{31}n_3)\frac{\Delta\Gamma}{\Delta x} + (E_{12}n_1 + E_{22}n_2 + E_{32}n_3)\frac{\Delta\Gamma}{\Delta y} + (E_{13}n_1 + E_{23}n_2 + E_{33}n_3)\frac{\Delta\Gamma}{\Delta z}\right]^{(b)} \\ + \left[(E_{11}n_1 + E_{21}n_2 + E_{31}n_3)\frac{\Delta\Gamma}{\Delta x} + (E_{12}n_1 + E_{22}n_2 + E_{32}n_3)\frac{\Delta\Gamma}{\Delta y} + (E_{13}n_1 + E_{23}n_2 + E_{33}n_3)\frac{\Delta\Gamma}{\Delta z}\right]^{(c)} \\ + \left[(E_{11}n_1 + E_{21}n_2 + E_{31}n_3)\frac{\Delta\Gamma}{\Delta x} + (E_{12}n_1 + E_{22}n_2 + E_{32}n_3)\frac{\Delta\Gamma}{\Delta y} + (E_{13}n_1 + E_{23}n_2 + E_{33}n_3)\frac{\Delta\Gamma}{\Delta z}\right]^{(d)}\end{array}\right\}_{6,10} \tag{7.4.16}$$

$$\left(\frac{1}{\Delta x}\right)_{6,10} = \left(\frac{\Delta y \Delta z}{\Delta\Omega}\right)_{6,10}, \quad \left(\frac{1}{\Delta y}\right)_{6,10} = \left(\frac{\Delta z \Delta x}{\Delta\Omega}\right)_{6,10}, \quad \left(\frac{1}{\Delta z}\right)_{6,10} = \left(\frac{\Delta x \Delta y}{\Delta\Omega}\right)_{6,10} \tag{7.4.17}$$

where $(\Delta x)_{6,10} = |x_6 - x_{10}|$, etc., $\Delta\Gamma$ being the subcontrol surface areas corresponding

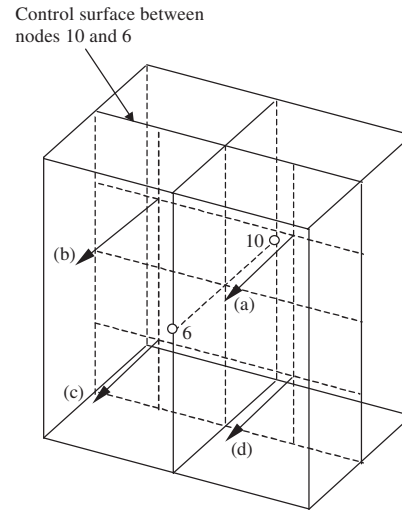

Figure 7.4.1 Control surface [normal vectors (a), (b), (c), (d)] between nodes 10 and 6 for the control volume containing node 10 of Figure 7.3.1.

to the normal vector components designated by (a), (b), (c), (d), and $(\Delta\Omega)_{6,10}$ represents the subcontrol volume for node 10 toward node 6 (Figure 7.3.2). As indicated in Section 7.2.1, if a cell is coincident with the x-, y-, or z-coordinate, then the left-hand side quantities in (7.4.17) must be used. However, the right-hand side quantities are used for the directions in which the coordinate components are zero to avoid singularities.

Similarly, we compute the right-hand side of (7.4.14) as in (7.4.10). The final form of the FDV/FVM equations is similar to (7.4.12) corresponding to the two interior nodes 10 and 11 (Figures 7.3.1 and 7.4.1).

It should be noted that the node-centered scheme described above is capable of accommodating any arbitrary unstructured grid system. Recall that in FDV equations, all physical aspects of the flow for all speed regimes have been accommodated as detailed in Section 6.5. Some applications of FDV methods via FVM/FEM are shown in Section 15.3.

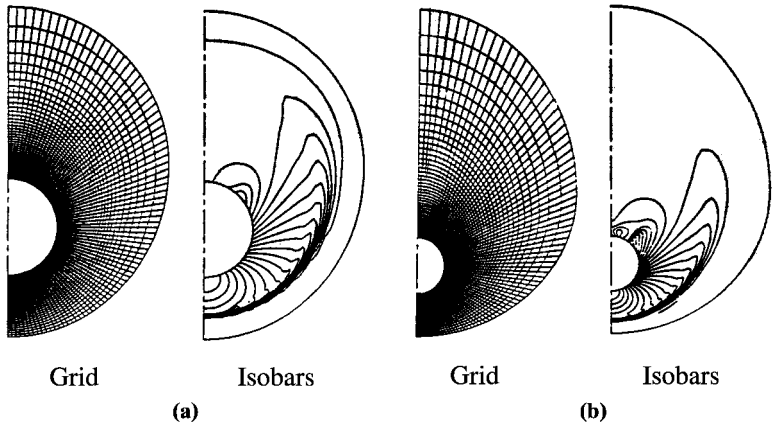

Figure 7.5.1 FVM/FDM solutions of Euler equations for flows over a circular cone [Siclari and Jameson, 1989]. **(a)** Euler grid and computed isobars for a 20° circular cone at $M_\infty = 2.0$, $\alpha = 25°$. **(b)** Euler grid and computed isobars for a 10° circular cone at $M_\infty = 2.0$, $\alpha = 25°$.

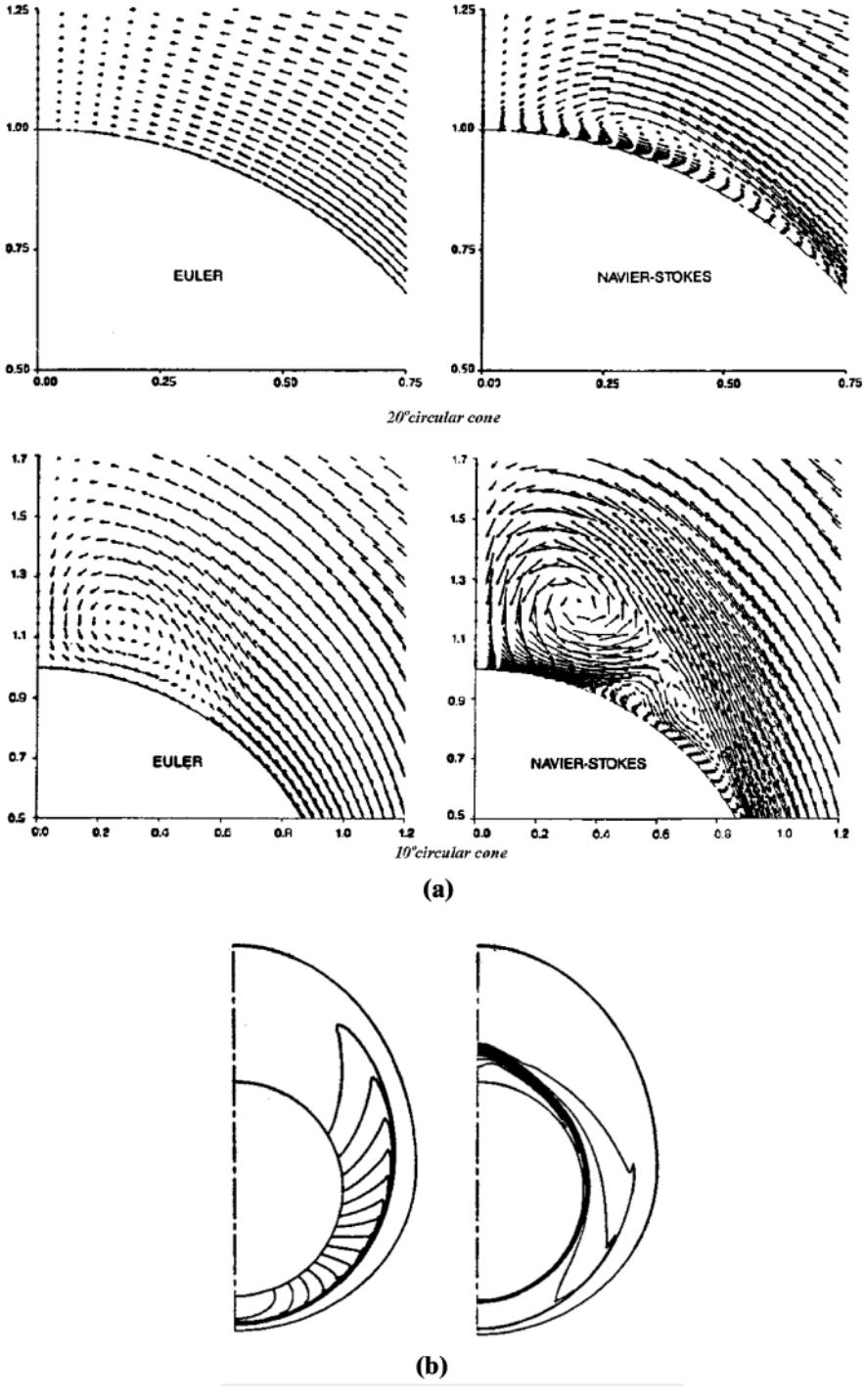

Figure 7.5.2 FVM/FDM solutions of Navier-Stokes system of equations for flows over a circular cone [Siclari and Jameson, 1989]. **(a)** Comparison of Euler and Navier-Stokes crossflow velocity vectors for a 10° and 20° circular cones at $M_\infty = 2.0, \alpha = 25°$. **(b)** Computed Navier-Stokes isobars and entropy contours for a 10° circular cone at $M_\infty = 7.95, \alpha = 12°, \text{Re} = 3.6 \times 10^6$.

7.5 EXAMPLE PROBLEMS

(1) Solution of Euler Equation Using FVM/FDM

The work presented here is reported by Siclari and Jameson [1989] on a node centered, finite volume, central difference scheme to solve the Euler equations. High-speed flows over a circular cone using spherical coordinates are investigated with FVM/FDM. To expedite the solution convergence, they used multigrid methods, which will be discussed in Section 20.2.

Figure 7.5.1a shows the (81×50) grid for a 20° circular cone with $M_\infty = 2.0$ and the cone angle of $\alpha = 25^\circ$. The resulting isobar solution shows that a weak crossflow shock occurs on the lee side of the cone with attached flow.

The geometry and discretization (81×50) for a 10° circular cone ($M_\infty = 2.0, \alpha = 25^\circ$) and the resulting isobar distributions are shown in Figure 7.5.1b. In this example, a strong crossflow shock develops on the lee side, resulting in shock-induced separation.

(2) Solution of Navier-Stokes System of Equations Using FVM/FDM

Siclari and Jameson [1989] solved the same problem above for the case of viscous flows. This requires additional attention, providing refined discretization, and higher order artificial dissipation as discussed in Section 6.3.

With the grid (81×68), the computed results are displayed in Figure 7.5.2a, compared with the case of inviscid flow. For the 20° cone, the Euler solution shows attached flow, whereas the Navier-Stokes solution shows a small separation. The Euler solution for the 10° cone shows a shock vorticity induced separation. The Navier-Stokes solution shows a more complex separated flow pattern including primary, secondary, and tertiary vortices.

Figure 7.5.2b shows the computed isobars and entropy contours. The leeside boundary layer separates at this incidence as indicated by the entropy contours.

7.6 SUMMARY

In this chapter, it has been shown that any finite difference schemes can be implemented in FVM with either structured or unstructured grids. There are two advantageous features in FVM: (1) Physically, the conservation of mass, momentum, and energy is assured in the formulation itself; and (2) Numerically, unstructured grids and arbitrary geometries are accommodated without coordinate transformation.

The conclusion appears to be that FVM is preferred to FDM for arbitrary geometries. For structured grids, however, such conclusion is premature. Personal preferences may persist for many years to come. The final outcome may be determined by convenience in applications associated with computing techniques from the viewpoints of data structure managements, which will be discussed in Chapter 20.

REFERENCES

Ni, R. N. [1982]. A multiple grid scheme for solving the Euler equations. *AIAA J.*, 20, 11, 1565–71.

Rizzi, A. W. and Inouye, M. [1973]. Time split finite volume method for three-dimensional blunt-body flows. *AIAA J.*, 11, 11, 1478–85.

Siclari, M. J. and Jameson, A. [1989]. A multigrid finite volume method for solving the Euler and Navier-Stokes equations for high speed flows. AIAA paper, AIAA-89-0283.